ELSEVIER

Chemical Engineering Journal 66 (1997) 207–215

Chemical Engineering Journal

New stochastic particle dispersion modeling of a turbulent particle-laden round jet

Jianren Fan *, Xinyu Zhang, Lihua Chen, Kefa Cen

Department of Energy Engineering, Zhejiang University, Hangzhou, People's Republic of China

Received 19 July 1996; accepted 3 January 1997

Abstract

A modified model for particle–eddy interaction in two-phase turbulent flows is proposed to account for the turbulent dispersion of particles in a turbulent flow. In order to validate the proposed model, the structure of a turbulent, particle-laden, round jet, injected into a still environment, is studied both theoretically and experimentally. The numerical results show good agreement with the experimental data. © 1997 Elsevier Science S.A.

Keywords: Stochastic model; Particle-laden jet; Particle dispersion; Numerical simulation; LDA measurement; LDM measurement

1. Introduction

Turbulent particle-laden round jets are found in many industrial applications such as coal combustion systems, cyclone separators, and classifiers. The presence of particles, even if their volume fraction is minute, can have a pronounced effect on the structure of the underlying turbulent gas flow field. Therefore, the primary problem in analyzing the gas-particle flow lies in treating the coupling of mass, momentum, and energy between two phases. In view of this, the two categorical approaches for predicting gas-particle flow are Eulerian and Lagrangian. In the Eulerian approach the two phases are considered to be separate interpenetrating continua, and separate (but coupled) equations of motion are solved for each phase. Recent models of this type are those of Elghobashi and Abou-Arab [1], Chen and Wood [2], Besnard and Harlow [3], Drew [4], Abou-Arab and Roco [5], Hwang and Shen [6,7]. In the Eulerian approach, microscopic effects occurring on the scale of the particle size, such as turbulent transport or particle–wall collisions, must be introduced through more or less sophisticated models. This method may be preferably used for dense two-phase flows, for example, in fluidized beds or two-phase flows with phase transition, e.g. from bubbly flow to mist flow. In the Lagrangian approach the dispersed phase is treated by solving Lagrangian equations for the trajectories of a statistically significant sample of individual particles, while the gas phase is treated as a continuum in the Eulerian approach. The two-way coupling between both phases is also accounted for [8]. The Eulerian/ Lagrangian approach allows an easy implementation of physical effects occurring on the scale of the particle size as, for example, particle–particle interactions and particle–wall collisions. Furthermore, numerical diffusion in the calculation of the dispersed phase is avoided, and a spectrum of the particle size can easily be simulated with less computational effort as compared to the Eulerian approach, where each size class has to be considered separately by solving one set of equations. The key element of the Eulerian/ Lagrangian approach is how it takes account of the effects of turbulent fluctuations on particle drag and dispersion, as well as the effects of particles on turbulence properties of the gas phase. One approach to modeling particle dispersion is to regard the particles as a gaseous species and use Fick's law, namely, an effective diffusion velocity [9] or diffusion "force" [10] in the particle motion equation, which is dependent on the particle concentration gradient. Since Fick's law is used in this approach to describe the turbulent diffusion of the particles, an effective diffusion coefficient must be chosen for which no reliable information is currently available. Another approach to modeling the particle dispersion process is to treat the turbulent flow as a random field. This is known as the stochastic particle dispersion model. Several stochastic particle dispersion models have been proposed. Yuu et al. [11] used a stochastic dispersion model, which employs empirical correlation of mean and turbulent properties, to analyze their measurements of particle dispersion in

* Corresponding author. Fax: +86 571 7951358.

PII S1385-8947(97)00006-5

jets. Gosman and Ioannides [12], Shuen et al. [13], Mostafa et al. [14], Berlemont et al. [15] and Sommerfeld [16] described several more comprehensive approaches, predicting both flow properties (using a k–ε model) and dispersion. The motion of the particles is traced as they interact with a succession of turbulent eddies, each of which is assumed to have constant flow properties. The effects of interphase slip and turbulent fluctuation are considered, using random sampling for turbulence properties in conjunction with random-walk computations for particle motion. However, because the turbulent movement of gas flow is a result of a random superposition of three fluctuation elements (i.e. different frequency, different amplitude, and different direction), it is oversimplifying to assume constant flow properties of a turbulent eddy.

In order to consider the turbulent dispersion of particles simply and completely, based on Gosman's approach, the present work reveals a new stochastic particle dispersion model to describe gas-particle turbulent flows. In this model, the continuous phase (gas phase) was described by the Eulerian formulation and a k–ε turbulence model was employed to find mean and turbulent properties of the continuous phase. The particle properties (velocity and trajectory) were then described by a Lagrangian approach, and computed using the mean velocity and turbulent fluctuation velocity of the gas phase. The gas turbulent fluctuating velocity in each eddy was simulated as a random Fourier series dependent on fluctuation frequency and the spectrum of turbulence. Therefore, the turbulent properties are assumed not to be uniform within each eddy. Thus, it is more consistent with the realistic situation of turbulent flows. On the other hand, mean dispersion properties of particle phase were obtained by averaging over a statistically significant number of particle trajectories. Also, the two-way coupling between both phases was accounted for in the present proposed model, in order to consider the momentum interchanges between gas and particle phases.

To validate the proposed numerical model and method, it is inevitable to compare the numerical results with detailed experimental studies obtained by applying modern measuring techniques for flow diagnostics. The present study provides detailed experiments of a turbulent axisymmetric gaseous jet laden with spherical nonuniformly sized solid particles in order to allow the validation of numerical predictions. Different flow conditions with varying particle loading ratios and initial gas phase velocities at the nozzle exit were considered. The present experiments included the velocities of both phases, which were measured using a phase discriminating laser-Doppler anemometer, and particle concentration and particle Sauter mean diameter, which were measured using a laser diffraction instrument. Furthermore, numerical predictions based on the proposed model were performed, and the results were compared with the measurements.

2. Mathematical model

The particle-laden round jet injected vertically into still air can be modeled as a steady axisymmetric flow. Mean quantities of the gas phase are found by solution of the governing equations for conservation of mass and momentum together with second order turbulent equations for turbulence kinetic energy k and its rate of dissipation ε, taking into account the source terms resulting from the momentum exchange with the dispersed phase. The general form of the elliptic differential equations for an axisymmetric flow is given by Eq. (1), and the source terms of the gas phase, S_Φ, the dispersed phase, $S_{\Phi,p}$, and the effective viscosity, Γ_Φ, are summarized in Table 1 for the different variables, Φ.

$$\frac{\partial}{\partial x}(\rho U\Phi)+\frac{1}{r}\frac{\partial}{\partial r}(\rho rV\Phi)-\frac{\partial}{\partial x}\left(\Gamma_\Phi\frac{\partial\Phi}{\partial x}\right)-\frac{1}{r}\frac{\partial}{\partial r}\left(r\Gamma_\Phi\frac{\partial\Phi}{\partial r}\right)=S_\Phi+S_{\Phi,p} \quad (1)$$

Table 1
Terms in the general equation

Φ	Γ_Φ	S_Φ	$S_{\Phi,p}$
1	–	0	0
U	μ_{eff}	$-\frac{\partial p}{\partial x}+\frac{\partial}{\partial x}\left(\mu_{eff}\frac{\partial U}{\partial x}\right)+\frac{1}{r}\frac{\partial}{\partial r}\left(\mu_{eff}r\frac{\partial V}{\partial x}\right)$	$S_{u,p}$
V	μ_{eff}	$-\frac{\partial p}{\partial r}+\frac{\partial}{\partial x}\left(\mu_{eff}\frac{\partial U}{\partial r}\right)+\frac{1}{r}\frac{\partial}{\partial r}\left(\mu_{eff}r\frac{\partial V}{\partial r}\right)-2\mu_{eff}\frac{V}{r^2}$	$S_{v,p}$
k	$\frac{\mu_{eff}}{\sigma_k}$	$G_k-\rho\varepsilon$	$S_{k,p}$
ε	$\frac{\mu_{eff}}{\sigma_\varepsilon}$	$\frac{\varepsilon}{k}(C_1G_k-C_2\rho\varepsilon)$	$S_{\varepsilon,p}$

$$G_k=\mu_{eff}\left\{2\left[\left(\frac{\partial U}{\partial x}\right)^2+\left(\frac{\partial V}{\partial r}\right)^2+\left(\frac{V}{r}\right)^2\right]+\left(\frac{\partial U}{\partial r}+\frac{\partial V}{\partial x}\right)^2\right\}$$

$\mu_{eff}=\mu+\mu_t$, $\mu_t=C_\mu\rho\frac{k^2}{\varepsilon}$, $C_\mu=0.09$, $C_1=1.44$, $C_2=1.92$, $\sigma_k=1.0$, $\sigma_\varepsilon=1.3$

Boundary conditions are required for the above equation and, wherever possible these are obtained from the measurements. The solution domain conforms to a symmetrical half section of the enclosures considered. In all cases, computations commenced at a downstream distance of 0.05 nozzle diameter (2 mm from the nozzle exit) where measured mean and fluctuating velocity profiles for both gas and particles are available. Consistent with the k–ε model, the initial profile for the turbulence energy dissipation rate was obtained in terms of the measured kinetic energy of turbulence k, shear stress τ (or $-\rho\overline{u'v'}$), and axial velocity gradient $\partial U/\partial r$, namely

$$\varepsilon = C_\mu \rho \frac{k^2}{\mu_t} \text{ and } \mu_t = \frac{\tau}{\partial U/\partial r} = \frac{-\rho\overline{u'v'}}{\partial U/\partial r} \tag{2}$$

At the axis of symmetry (the centerline of the jet), the boundary condition is of the form $\partial\Phi/\partial r = 0$. At the solid walls, the velocities are assumed to be zero, and these no-slip boundary conditions are appropriate for the gas and particle phase. These equations, called "wall functions", are introduced and used in finite difference calculations at near-wall points [21]. At the exit, all gradients are assumed to be zero [21], and this assumption had a negligible influence on the upstream flow.

The resulting set of equations is solved by using a finite volume discretization scheme and applying an iterative solution procedure based on the SIMPLE algorithm [17]. In order to accelerate the rate of convergence, a multigrid scheme was implemented. For the present case, three grid levels with 48×36, 96×70, 200×100 control volumes in the axial and radial directions, respectively, were used. In the streamwise direction, the computational domain was extended up to 1.2 m downstream of the inlet. The radial width of the computational domain was extended up to the confinement wall, as described in the experimental setup.

The dispersed phase was treated by solving Lagrangian equations for the trajectories of a statistically significant sample of individual particles parcels, representing a number of real particles with the same properties, as they move away from the injector and encounter a random distribution of turbulent eddies. The representation of the particles by parcels was used in order to allow the consideration of the particle size distribution and to simulate the appropriate particle mass flow rate at the injection locations. In order to guarantee a good statistical result, eight thousand parcels were traced through the flow field. Assumptions for particle parcels trajectory calculations are typical of the analysis of dilute particle-laden flows: drag is treated empirically, since $\rho_p/\rho > 1000$ for the present tests, the effects of virtual mass, Basset history force and Magnus force are neglected, assuming a quasisteady flow for spherical particles, and particle collision is neglected. With these assumption, the equation of motion for the kth computational particle parcels in the ith direction is given by:

$$\frac{dx^k_{p,i}}{dt} = u^k_{p,i} \tag{3}$$

$$\frac{du^k_{p,i}}{dt} = \left(\frac{3\rho C^k_D}{4d^k_p\rho_p}\right)(u_{g,i} - u^k_{p,i})\,|\boldsymbol{u}_g - \boldsymbol{u}^k_p| + g_i \tag{4}$$

The drag coefficient was determined from the following correlation:

$$C^k_D = \frac{24}{Re^k_p}\left[1 + 0.15(Re^k_p)^{0.687}\right] \qquad Re^k_p < 1000$$

$$C^k_D = 0.44 \qquad Re^k_p \geq 1000$$

with:

$$Re^k_p = \frac{d^k_p|\boldsymbol{u}_g - \boldsymbol{u}^k_p|}{\nu}$$

As mentioned in the introduction, the effect of the turbulence on the particle motion is simulated here by a new stochastic approach. The instantaneous gas phase velocity $u_{g,i}$ in Eq. (4) is expressed by the time average gas phase velocity $U_{g,i}$, which is obtained from the solution of the mean flow equation of the gas phase (Eq. (1)), and the fluctuating velocity $u'_{g,i}$:

$$u_{g,i} = U_{g,i} + u_{g,i}' \tag{5}$$

The gas phase fluctuating velocity $u'_{g,i}$ in a particular eddy is simulated by a random Fourier series, namely:

$$u'_{g,i} = \sum_{n=1}^{n=10} R_1 U_{m,i}\cos(\omega_n t - R_2\alpha) \tag{6}$$

where the random variables R_1 and R_2 are sampled from a uniform probability distribution between 0 and 1. α is the initial fluctuating phase, and the frequency ω_n is picked from a Gaussian distribution with a standard deviation of unity. For the incompressible, isotropic turbulent flow field, the fluctuating amplitude $U_{m,i}$ can be given as

$$U_{m,i} = \left(\int_0^\infty E(K)\,dK\right)^{1/2} \tag{7}$$

where $E(K)$ is the energy spectrum, and K is the wave number. The energy spectrum of the round jet was measured by Laurence [18]. Based on the experimental data of Laurence, the energy spectrum $E(K)$ is given by

$$E(K) = 16\left(\frac{2}{\pi}\right)^{1/2} K^4 e^{-2K^2} \tag{8}$$

The comparison of the probability distribution functions for the velocity fluctuations in the gas phase at several axial and radial positions, which are calculated by the Fourier representation reproduces (Eq. (6)) and measured by the present experiment (Case 1), is shown in Fig. 1. It is noticeable that the agreement between the predictions and measurements is reasonable good.

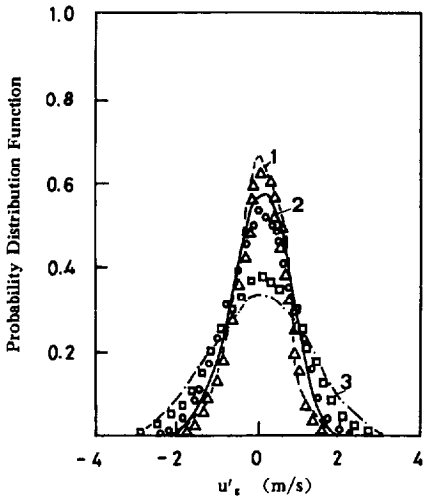

Fig. 1. Comparison of the predicted and measured probability distribution functions for the velocity fluctuations in the gas phase for Case 1, Curve 1 (△), $x/D_0=15$, $r/r_0=0$; Curve 2 (○), $x/D_0=20$, $r/r_0=0$; Curve 3 (□), $x/D_0=20$, $r/r_0=1.5$.

This gas phase fluctuating velocity $u'_{g,i}$ is assumed to influence the particle motion during a given time period, the interaction time before a new fluctuating velocity is sampled. The interaction time τ_{int} is the minimum of turbulent eddy lifetime (τ_e) and the residence time of the particle in the eddy (τ_r) reported by Gosman and Ioannides [12]. It is assumed that the characteristic length of the turbulent eddies is that of the mean integral length scale l_e, given by:

$$l_e = C_\mu^{3/4}\frac{k^{3/2}}{\varepsilon} \tag{9}$$

The eddy lifetime is obtained from

$$\tau_e = \frac{l_e}{u'_{g,i}} \tag{10}$$

The residence time of the particle in the eddy, e.g. the time for a particle to pass through that eddy, is estimated from the following solution of a simplified and linearized form of equation of motion of the particle [12]:

$$\tau_r = -\tau\ln\left(1.0-\frac{l_e}{\tau|u_g-u_p^k|}\right) \tag{11}$$

where τ is the particle relaxation time, defined as $\tau=\frac{4}{3}\rho_p d_p/(\rho C_D|u_g-u_p^k|)$. Hence,

$$\tau_{int} = \min(\tau_e,\tau_r) \tag{12}$$

For each particle parcel, the equation of motion is integrated over as many time increments as required for the particle parcels to traverse the required distance. When a sufficiently large number of particle parcels is tracked, their averaged behavior should represent the cloud and yield the effects of the gas turbulence characteristics on the motion of the particles.

The interaction between particles and the gas phase yield source terms in the governing equation for conservation of momentum and in the model equations for k and ε when turbulence modulation is considered. The source terms in the U and V equations are found by computing the net change in momentum along each particle parcel trajectory k and passing through the computational cell j:

$$S_{u,p} = \sum_{k=1}^{n} n^k m_p^k (u_{p,in}^k - u_{p,out}^k)/\Delta V_j \tag{13}$$

$$S_{v,p} = \sum_{k=1}^{n} n^k m_p^k (v_{p,in}^k - v_{p,out}^k)/\Delta V_j \tag{14}$$

where n^k is the number of the kth computational particle parcel per unit time along the particle trajectory. m_p^k is the kth particle parcel mass. $u_{p,in}^k$, $v_{p,in}^k$ and $u_{p,out}^k$, $v_{p,out}^k$ are the velocities of the kth particle parcel when traversing into a given computational cell boundary (subscript "in") and traversing out this computational cell boundary (subscript "out") during integration of the particle equations. ΔV_j is the volume of computational cell j. Source terms in the governing equations for turbulence quantities $S_{k,p}$ and $S_{\varepsilon,p}$ were derived following conventional procedures given by Grancher [19].

$$S_{k,p} = (\overline{uS_{u,p}} - \bar{u}\,\overline{S_{u,p}}) + (\overline{vS_{v,p}} - \bar{v}\,\overline{S_{v,p}}) \tag{15}$$

$$S_{\varepsilon,p} = C_{\varepsilon 3}\frac{\varepsilon}{k}S_{k,p} \tag{16}$$

where $C_{\varepsilon 3}=1.87$, using the data of Ref. [13].

The equivalent finite difference form of the gas phase general equation (Eq. (1)) is readily obtained by a cell or volume integration following the rules and guidelines in Patankar [17]. A staggered convention is adopted, whereby velocity components are stored at locations half-way between adjacent grid points, whilst scalar fields (e.g. pressure, turbulent kinetic energy and its dissipation rate) reside at the grid point, as shown in Fig. 2. It should be noted that if the particle parcels do not lie directly on grid points, then the area-weighted-mean interpolations are required to estimate the gas phase velocities $U_{g,P}$ and $V_{g,P}$ at the location P, at which the particle is located.

$$U_{g,P} = (U_{i,j}A_2 + U_{i+1,j}A_1 + U_{i,j+1}A_4 + U_{i+1,j+1}A_3)/\sum_{i=1}^{4}A_i \tag{17}$$

$$V_{g,P} = (V_{i,j}B_2 + V_{i+1,j}B_1 + V_{i,j+1}B_4 + V_{i+1,j+1}B_3)/\sum_{i=1}^{4}B_i \tag{18}$$

where A_i and B_i are element areas shown in Fig. 2.

3. Experimental method

The experimental setup for the particle-laden jet is shown schematically in Fig. 3. The particle-laden round jet was directed vertically downward within a screened enclosure, of

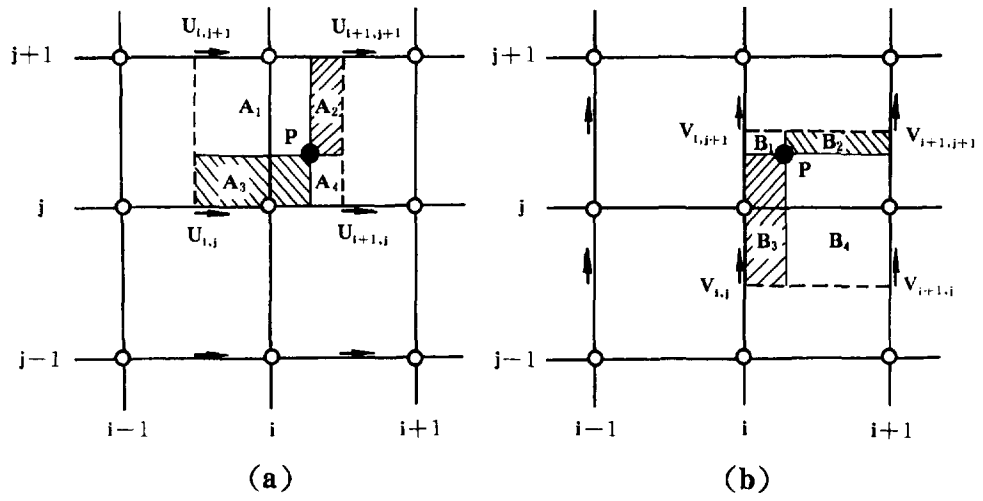

Fig. 2. Staggered-difference grid and the area-weighted-mean interpolations of the gas phase velocities. (a) Axial velocity component interpolation; (b) radial velocity component interpolation.

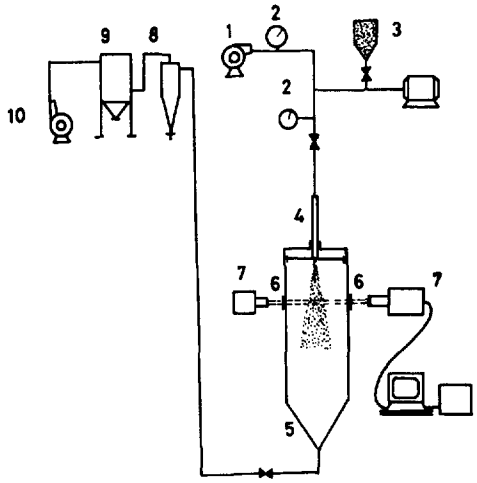

Fig. 3. Experimental set-up. 1, blower; 2, flowmeter; 3, powder feeder; 4, nozzle; 5, chamber; 6, optical window; 7, LDA; 8, cyclone; 9, dust-remover; 10, exhaust blower.

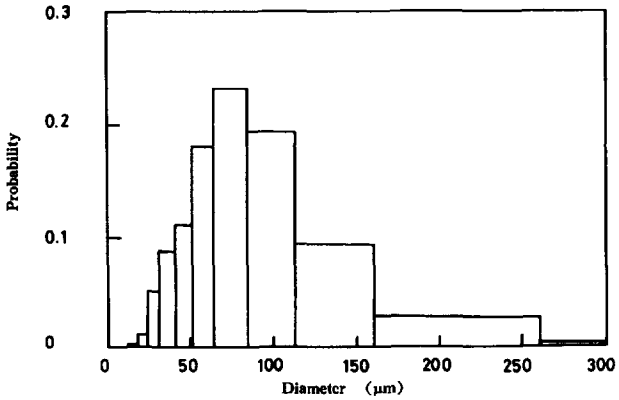

Fig. 4. Particle size distribution.

diameter 600 mm. The jet tube had an inside diameter of 40 mm. The injection tube was 100 diameters long to provide a fully developed turbulent pipe flow at the jet inlet. The boundary at the jet inlet plane was a wall. There was not any secondary or entrainment stream at this plane. A fixed height optical measurement station was provided with the capability to move the entire assembly of the feeder/shaker and jet tube vertically in order to map the whole flow field. The air and particles were sucked to the bottom of the chamber by another blower. Silica particles were separated by the cyclone and the dust remover and were weighted by a load cell set under the receiver tank.

Experiments were performed using silica gel powder at a material density of 1250 kg m^{-3}. Particle size distribution was measured using a Malvern laser diffraction instrument with a sample of more than 2000 particles for each size group. The representative particle size distribution curve is shown in Fig. 4. The initial particle mass loading ratio, ϕ_0, defined as the ratio of the total solid mass flow rate to the mass flow rate of the air at the nozzle exit, was changed from 0.22 to 0.80. Details of four test conditions are summarized in Table 2.

Mean and fluctuating gas velocities were measured with a single-channel, frequency-shifted 15 mw He–Ne laser-Doppler anemometer (LDA) having an ellipsoidal measuring volume (98 μm in diameter, 450 μm long) with a fringe spacing of 3.13 μm. For the measurement of the air velocity the flow was seeded with small spherical glass beads with sizes between 0 and 8 μm and a mean diameter of 4.3 μm. In order to guarantee that only seeding particles with a size less than 4 μm are sampled for obtaining the air velocity a discrimination procedure based on the phase between the two signals was used. Uncertainties in mean and fluctuating gas velocity are estimated to be less than 6% and were repeatable within 3%.

Mean and fluctuating particle velocities were measured using the same LDA, but with no seeding particles and low detector gain so that only strong scattering signals from test particles were observed. Mean and fluctuating velocities found by the LDA were checked by calibration at several conditions, indicating uncertainties less than 8% for results reported here. Particle concentration and particle size distributions were measured with a Malvern laser diffraction instrument whose method of operation is based on Fraunhofer

Table 2
Experimental flow conditions at 0.05 D_0 downstream of nozzle exit

Parameter	Single phase air jet	Particle-laden jet		
		Case 1	Case 2	Case 3
Gas phase (air)				
Centerline velocity, $U_{g,0}$ (m s^{-1})	20	20	20	30
Exponent, n, of power law velocity profile, ($U_g/U_{g,0}=[1-(2r/D_0)^{1/n}]$)	6.80	6.61	6.61	6.61
Density, ρ_g (kg m^{-3})	1.178	1.178	1.178	1.178
Reynolds number, Re	53 571	53 571	53 571	80 357
Solid phase (silica particles)				
Centerline velocity, $U_{p,0}$ (m s^{-1})	–	19.1	19.1	28.8
Particle mean diameter, d_p (μm)	–	72	72	72
Particle loading ratio, ϕ_0	–	0.22	0.80	0.80

diffraction theory. However, the laser diffraction method (LDM) only provides line integrals of the particle concentration and the particle size along all straight lines intersecting the measured cross-section. In order to obtain the real particle concentration and particle size distributions in the measured cross-section an effective data transform procedure must be performed, which has been developed by Fan et al. [20]. Due to the uncertainties in the determination of the cross-section of the control volume the measured concentration was corrected using the global mass balance.

Therefore, the total particle mass flow rate at the inlet was obtained by integrating the mass flux profile. In comparison with the global mass flow rate obtained by weighing the particles collected during a certain time period in the cyclone separator, a correction factor was determined and applied to the concentration measurements in the whole measured cross-section. By integrating the concentration profiles it was calculated that the particle mass flow rate at the considered cross sections deviated from the mass flow rate at the inlet to ±8%.

4. Result and discussion

The results presented here were obtained using 100 lateral nodes to span the flow domain between the centerline of the jet and its outer edge. The dispersed phase was computed using a Runge–Kutta method employing no less than 8000 particle parcels. Furthermore, a continuous distribution of particle sizes was represented by a discrete distribution of a few different particle diameters.

The experimental results are plotted in a dimensionless from vs. r/r_0. In this way the jet spreading can be easily seen from the axial profiles of the mean axial velocities. All quantities except mean axial gas velocities are normalized by the local mean centerline values. The mean axial gas velocities are normalized by the initial jet centerline velocity at the nozzle exit, $U_{g,0}$.

Fig. 5 shows the measured and predicted distributions of mean velocity and rms axial velocity of both phases and the particle concentration with the particle loading ratio $\phi_0=0.22$ (Case 1). Agreement between predictions and measurements is reasonable good for the gas phase and particle phase. In order to assess the improvement achieved by the proposed modification, the predictions with the stochastic model developed by Shuen et al. [13] are also given in Fig. 5. It can be seen that the present model and Shuen's model yield nearly the same results for gas quantities. However, for particle quantities the present model provides good predictions compared with the experimental data, whereas the Shuen's model performs quite poorly for the particle flow properties. According to the latter, a particle moves radially due to its mean and fluctuation radial velocities, both of which are very small compared with the axial component. This might explain the narrow distribution of particle mean axial velocity and concentration predicted by Shuen's model.

The predicted and measured centerline velocity decay of the gas phase is illustrated in Fig. 6 for three test conditions. It is noted that the gas velocity decay of the particle-laden jet is slower than that of a single phase jet. The presence of the dispersed phase causes the jet to be more coherent. Because of the slow decay of the particle mean velocity, there is momentum transfer from the dispersed phase to the gas which causes an increase in the latter velocity compared with the corresponding single phase values. This change in the gas flow properties could also be attributed to the gas turbulence attenuation caused by the particles. Gas turbulence attenuation causes a reduction in the jet spreading rate that results in less decay of the gas centerline velocity. Fig. 6 also shows a more slower decay of the gas centerline velocity with the increasing particle loading ratio ϕ_0, which might be explained by the fact that both the momentum transfer and turbulence modulation are proportional to ϕ_0. Fig. 7 presents the centerline velocity decay of both phases for Case 1. Notice that from the end of the potential core on, because of the particles' inertia, the particulate phase velocity is higher than the gas phase velocity. The velocity slip between both phases exists, obviously.

In Fig. 8, detailed mean field properties for the single phase air jet and the particle-laden jet (Case 1) are plotted for $x/D_0=20$. It is shown that the gas phase diffuses quicker than the dispersed phase. The particle concentration vanishes at a radial distance of $r/r_0=4$ while the fluid spreads to at least

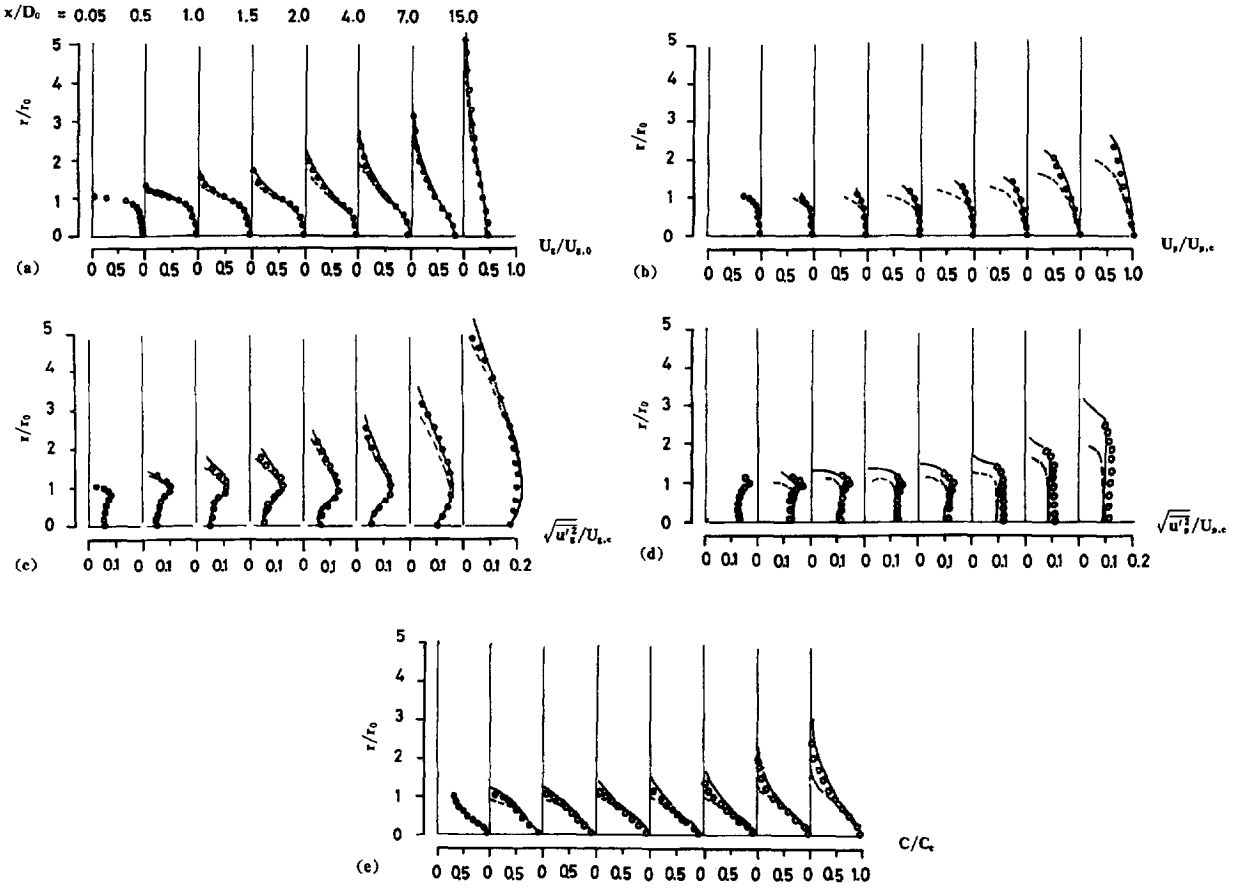

Fig. 5. Radial profiles of normalized gas phase axial velocity (a); particle phase axial velocity (b); gas phase axial turbulence kinetic energy (c); particle phase axial turbulence kinetic energy (d); particle phase concentration (e) for Case 1. (○, experimental data; —, predictions of present model; - - -, prediction of Shuen's model).

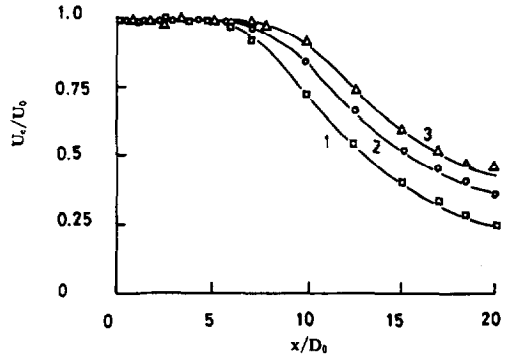

Fig. 6. Centerline gas phase velocity decay. Curve 1 (□), single phase air jet; Curve 2 (○), particle-laden jet for Case 1; Curve 3 (△), particle-laden jet for Case 2.

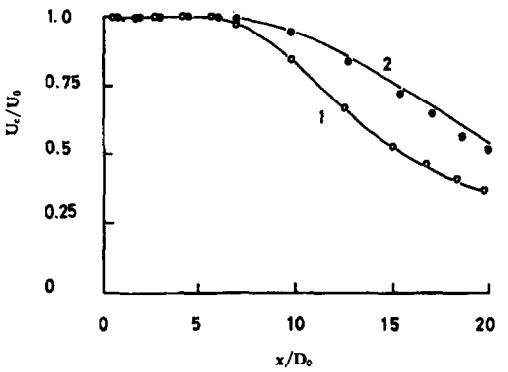

Fig. 7. Centerline velocity decay. Curve 1 (○) gas phase $U_{g,c}/U_0$; Curve 2 (●) particle phase $U_{p,c}/U_{p,0}$ for Case 1.

two times this distance. Conservation of momentum of each phase then results in the dispersed phase axial velocity being much higher than that of the gas phase, and in turn the particles continue to be a source of momentum for the gas phase. It is clear from Fig. 8 that the single phase air jet spreads more widely than the particle-laden jet, which reason has been discussed above. It can also be seen from Fig. 8 that the particle concentration is decaying much faster than the particle velocity. This means that the spreading of the dispersed phase dilutes the particle concentration but does not necessarily decelerate the particles.

Fig. 9 shows the predicted and measured particle concentration and particle mean diameter distributions for Case 2 and Case 3. The particle mean diameters at the jet edge are approximately 20% smaller than that at the jet centerline. It is evident that the larger particles disperse more slowly than the smaller particles, since dispersion is caused by drag forces of the gas on particles which vary strongly with particle size. On the other hand, these particle dispersions increase with the initial gas velocity at the jet exit.

The effect of the particles on the gas turbulence structure is shown in Fig. 10. Also shown for comparison is the single

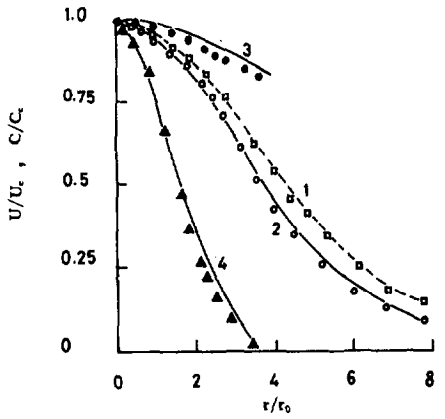

Fig. 8. Mean radial profiles. Curve 1 (□), mean velocity of single phase air jet; Curve 2 (○), mean gas phase velocity $U_g/U_{g,c}$; Curve 3 (●), mean particle phase velocity $U_p/U_{p,c}$; Curve 4 (▲) mean particle phase concentration C/C_c. $(x/D_0=20)$.

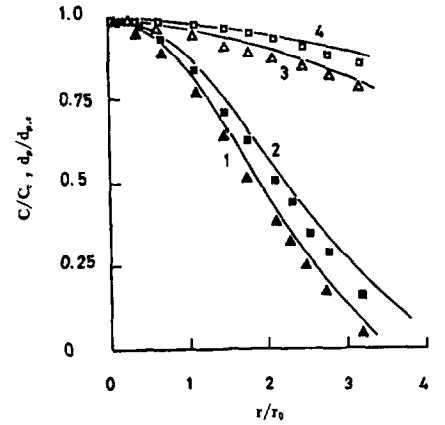

Fig. 9. Mean radial profiles. Curve 1 (▲), mean particle phase concentration C/C_c for Case 2; Curve 2 (■), mean particle phase concentration C/C_c for Case 3; Curve 3 (△), mean particle size $d_p/d_{p,c}$ for Case 2; Curve 4 (□), mean particle size $d_p/d_{p,c}$ for Case 3. $(x/D_0=20)$.

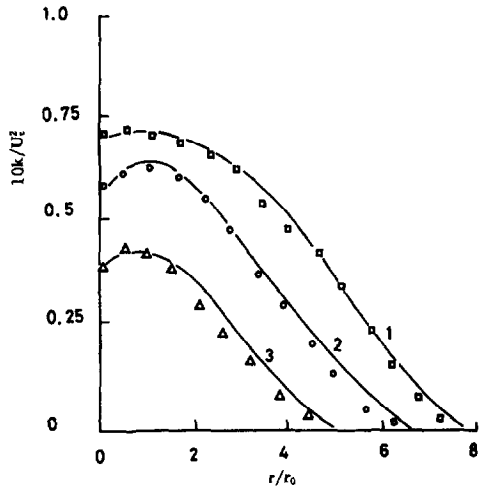

Fig. 10. Radial profiles of the turbulent kinetic energy. Curve 1 (□), single phase air jet; Curve 2 (○), particle-laden jet of Case 1; Curve 3 (△), particle-laden jet of Case 2. $(x/D=20)$.

phase air jet profile. One could observe some reduction in gas kinetic energy of turbulence caused by the particles. This reduction is more pronounced at higher particle loading. For Case 2 ($\phi_0=0.80$) the local turbulence intensity corresponds to a reduction of about 40% of the single phase value. This turbulence modulation is caused mainly by the fluctuating relative velocity between the particles and the carrier phase. Particles generally cause a reduction in the gas turbulence and an increase in the dissipation rate of that energy. The relative decrease in turbulence energy caused by the presence of the particles is well predicted.

5. Conclusion

The new stochastic particle dispersion model presented here allowed the correct simulation of turbulent, particle-laden, round jets and yielded good estimates of the flow and the turbulent dispersion for particle-laden jets.

A detailed data set is presented for gas and particle mean and fluctuating velocity measurements and particle concentration and particle size distributions within the developing region of a particle-laden, round jet. The effect of the particle mass loading ratio and the initial gas velocity at the nozzle exit on the gas phase flow properties is investigated. The higher particle mass loading ratio decreases the spreading and turbulence in the jet relative to the lower particle mass loading ratio. The data have also been used to assess the accuracy of the proposal stochastic particle dispersion model. Thus, this approach appears to be useful for a wide range of two-phase flows, and merits further development.

Acknowledgements

This project has been supported by the National Natural Science Foundation of the People's Republic of China.

Appendix A. Nomenclature

C	particle concentration (kg kg^{-1})
$C_\mu, C_1, C_2, C_{\varepsilon 3}$	coefficient in the turbulent model
C_D	drag coefficient
d_p	particle diameter (μm)
D_0	nozzle diameter (mm)
g	gravitational acceleration (m s^{-2})
k	kinetic energy of turbulence (m^2 s^{-2})
l_e	eddy size (m)
m_p	particle mass (kg)
n	particle number density (s^{-1})
p	static pressure (Pa)
R	random number
r	distance in the radial direction (m)
Re_p	particle Reynolds number
S	source term
t_{in}, t_{out}	times when the particle enters and leaves the gas phase control volume (s)

U,u',u	mean, fluctuating, and instantaneous velocity (m s^{-1})
$\boldsymbol{u}$	velocity vector (m s^{-1})
x	distance in the axial direction (m)
ΔV	control volume (m^3)

Greek letters

α	fluctuation phase (rad)
Γ_Φ	effective viscosity (m^2 s^{-1})
ε	kinetic energy dissipation rate (m^2 s^{-3})
μ	dynamic viscosity of the gas phase (kg m^{-1} s^{-1})
ν	kinematic eddy viscosity of the gas phase (m^2 s^{-1})
ρ	material density (kg m^{-3})
τ_e	turbulent eddy lifetime (s)
τ_r	residence time of the particle in the eddy (s)
τ_{int}	interaction time of particle (s)
$\sigma_k,\sigma_\varepsilon$	coefficient in the turbulence model
Φ	generic property
ϕ_0	particle loading ratio
ω	fluctuation frequency (Hz)

Subscripts

0	conditions at the nozzle exit
c	conditions at the jet centerline
g	gas phase
i	ith direction
p	particle phase

Superscripts

k	kth trajectory of a computational particle

References

[1] S.E. Elghobashi, T.W. Abou-Arab, Phys. Fluids 26 (1983) 931–943.
[2] C.P. Chen, P.E. Wood, Chem. Eng. Commun. 29 (1984) 291–300.
[3] D.C. Besnard, F.H. Harlow, Int. J. Multiphase Flow 14 (1988) 679–692.
[4] D.A. Drew, J. Fluids Eng. 112 (1990) 362–366.
[5] T.W. Abou-Arab, M.C. Roco, J. Fluids Eng. 112 (1990) 351–361.
[6] G.-J. Hwang, H.H. Shen, Int. J. Multiphase Flow 17 (1991) 45–57.
[7] G.-J. Hwang, H.H. Shen, Int. J. Multiphase Flow 19 (1993) 887–895.
[8] C.T. Crowe, M.P. Sharma, D.E. Stock, J. Fluids Eng. 99 (1977) 325–332.
[9] A.S. Abbas, S.S. Koussa, F.C. Lockwood, Proc. 18th Symposium (International) on Combustion, The Combustion Institute, Pittsburgh, PA, 1981, pp. 1427–1438.
[10] P.J. Smith, T.H. Fletcher, L.D. Smoot, Proc. 18th Symposium (International) on Combustion, The Combustion Institute, Pittsburgh, PA, 1981, pp. 1285–1293.
[11] S. Yuu, N. Yasukouchi, Y. Hirowawa, T. Jotaki, AIChE J. 24 (1978) 509–519.
[12] A.D. Gosman, E. Ioannides, AIAA Paper, 81-0323, 1981.
[13] J.-S. Shuen, A.S.P. Solomon, Q.-F. Zhang, G.M. Faeth, AIAA J. 23 (1985) 396–404.
[14] A.A. Mostaf, H.C. Mongia, V.G. McDonell, G.S. Samuelsen, AIAA J. 27 (1989) 167–183.
[15] A. Berlemont, P. Desjonqueres, G. Gouesbet, Int. J. Multiphase Flow 16 (1990) 19–34.
[16] M. Sommerfeld, Int. J. Multiphase Flow 18 (1992) 905–926.
[17] S.V. Patankar, Numerical Heat Transfer and Fluid Flow, Hemisphere Publishing Co., 1980.
[18] I.C. Laurence, NACA Report, N-1292, 1956.
[19] M.-S. Grancher, PhD Thesis, Faculté de Sciences de l'Université de Rouen, 1990.
[20] J. Fan, L. Zhang, H. Zhao, K. Cen, Expt. Fluids 9 (1990) 320–322.
[21] B.E. Launder, D.B. Spalding. Comput. Methods Appl. Mech. Eng. 3 (1974) 269.